Validation of Universal Cryogenic Flow Boiling Correlations in Thermal Desktop for Liquid Helium

Erin Tesny[1], Jason Hartwig[1], Vishwanath Ganesan[2], Issam Mudawar[2] and Mariano Mercado[1]
[1] NASA Glenn Research Center, 21000 Brookpark Rd, Cleveland, Ohio, 44135, USA
[2] 2Purdue University, West Lafayette, IN, 47907

Email: erin.m.tesny@nasa.gov

Abstract. Understanding two-phase cryogenic propellant behavior is key to enabling technologies for future spaceflight missions. Developing accurate models of two-phase flow phenomena, particularly in the current work, flow boiling in the heating configuration, is relevant to the propellant transfer process both in 1-g and microgravity. Currently there is a need for more accurate, direct cryogenic data anchored models for various boiling phenomena. Recently, universal correlations for cryogens flowing in heated tubes have been developed for a wide variety of fluids, thermodynamic conditions, and various regimes across the boiling curve, and have been patched to provide a smooth, continuous predictive curve. This paper describes implementation and validation of these correlations into Thermal Desktop to improve predictive performance, with a focus on liquid helium. Results from Thermal Desktop using both the built-in and new correlations are validated against a historical dataset of flow boiling experiments in the heating configuration using liquid helium. Based on results, the new correlations show a substantial improvement over the original built-in flow boiling correlations in Thermal Desktop in predicting the wall temperature as a function of preponderant parameters for this quantum fluid at temperatures greater than the lambda temperature, $T_\lambda = 2.17$K.

1. Introduction

The Flow boiling of cryogenic fluids is of particular interest to the design of future propellant storage and transfer systems. For example, in-space transfer lines that lack proper insulation are susceptible to heat leak that can result in flow boiling in the line. To accurately design transfer systems with two-phase flow, accurate models that can predict the rate of boiling and the resultant wall temperatures are required so that propellant and insulation mass can be minimized. Existing modeling tools predominately rely on flow boiling correlations developed for room temperature fluids and have been shown to generally be inaccurate when used for cryogens. The current work presented here validates newly developed universal cryogenic correlations in Thermal Desktop against a historical heated tube dataset for liquid helium (LHe), Giarrantano et al. [1]. The results compare the predicted wall temperatures using the universal correlations and using the built-in Thermal Desktop correlations.

2. Overview of New Universal Correlations

New universal cryogenic flow boiling correlations were developed and recently patched together in [2] to form a smooth, continuous boiling curve for predicting heat flux or heat transfer coefficient (HTC) from left-to-right on the boiling curve shown in Figure 1. Specific correlations were developed for the onset of nucleate boiling, subcooled or saturated nucleate boiling HTC, Departure from Nucleate Boiling (DNB) and Dryout-type critical heat flux (CHF) (or location of CHF), film boiling HTC for both Dispersed Flow Film Boiling (DFFB) and Inverted Annular Film Boiling (IAFB), and two-phase pressure drop [3-7]. To merge the pre-CHF with post-CHF correlations, a hyperbolic tangent function was used to "blend" the last pre-CHF HTC value ($h_{\text{tp,pre-CHF}}$) evaluated at the location just before CHF (z_{CHF}), to the post-CHF HTC values ($h_{\text{tp,post-CHF}}$) evaluated at locations for the entire post-CHF length ($z_{\text{CHF}} \leq z \leq L_{\text{H}}$) of the pipe. L_{H} is the heated length of the pipe [2]. This function is shown in Equation 1

where φ is the blending coefficient which determines the smoothness of the patched HTC ($h_{tp,patched}$) from the CHF location to the end of the heated length.

$$\frac{1}{h_{tp,patched}} = \frac{1}{h_{tp,pre-CHF}} + \frac{1+\tanh\left(\varphi\left(z-z_{CHF}\right)\right)}{2}\left(\frac{1}{h_{tp,post-CHF}} - \frac{1}{h_{tp,pre-CHF}}\right) \tag{1}$$

The final patched HTC, $h_{tp,patched}$, is then used in the post-CHF region. The blending coefficient, φ, was set to 5 for all runs. The complete, continuous boiling curve with blending applied is called "The Universal Correlations".
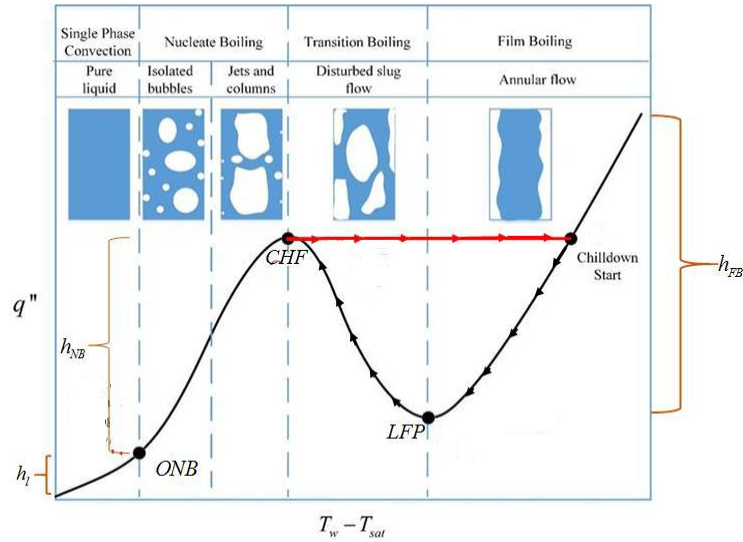

Figure 1: A typical boiling curve illustrating key regimes and transition points, taken from [8]

3. Thermal Desktop Model Description

3.1. Overview of Experimental Test Set Up

The experimental test set up was designed to observe LHe flow boiling in the heating configuration [1]. A constant heat flux was applied to the outside of a vertical stainless steel test section tube. The tube had a length 10 cm, wall thickness of 0.016 mm, and inner diameter 2.1 mm. Ten carbon resistance thermometers were placed along the outside of the wall to measure wall temperature. LHe was flowed through the tube as a constant heat flux was applied to the outside. The test matrix with the inlet and operating conditions for select runs from [1] is shown in Table 1. This includes the thermodynamic equilibrium quality at inlet ($x_{e,in}$), bulk fluid temperature at the inlet (T_{in}), inlet pressure (P_{in}), wall heat flux (q''), mass velocity (G), and experimental location of CHF (z_{CHF}) if there exists one. The last column of this test matrix denotes the number of points of useful experimental wall temperature (T_w) available for each run.

Table 1: Inlet and operating conditions of select Giarrantano et al. [1] runs

Run # from [1]	$x_{e,in}$	T_{in} (K)	P_{in} (MPa)	q'' (W/m²)	G (kg/m²s)	z_{CHF} (mm)	T_w Data Points
Figure 3 Run 1	-0.00784	4.3	0.1088	2280	48	86.03	8
Figure 3 Run 2	-0.00750	4.3	0.1088	1800	48	-	10
Figure 4	-0.00750	4.3	0.1088	2570	113	96.8	9
Figure 5	-0.00402	4.31	0.1088	2620	294	-	10

Figure 6	-0.0530	4.24	0.1116	620	73	-	4
Figure 7	-0.0190	4.5	0.1301	5300	636	35.7	3
Figure 8	-0.114	4.4	0.1370	2840	153	86.2	5
Figure 9	-0.0792	4.5	0.1389	2530	76	66.1	5
Figure 9	-0.0679	4.53	0.1413	1750	76	-	
Figure 10	-0.4652	4.8	0.1755	1650	80	66.3	

3.2. General Model Description

The Thermal Desktop model consists of a single pipe composed of fluid lumps and solid nodes to represent the fluid and wall, respectively. Each test point consists of a single fluid lump connected to a solid node via a tie that governs the convective heat transfer. Solid nodes are connected via conductors that govern the axial conduction along the pipe wall. The material properties of stainless steel are applied to the solid wall nodes. The Thermal Desktop SINDA/FLUINT solver uses an iterative scheme, so 10 nodes were used in all runs to match the number of wall thermocouples in the test set up. A constant heat flux is applied to the wall nodes to simulate the heating element.

As shown in Table 2, the "Built-In Correlations" in Thermal Desktop consists of several existing correlations depending on equilibrium quality and wall superheat [9]. A full accounting of these correlations and the logic behind them can be found in [10]. At low wall superheats, below the CHF temperature, T_{CHF}, the temperature at which the critical heat flux is exceeded, the code uses either the correlation by Chen [11] or, at high flow qualities, an interpolation between Chen's correlation and the single-phase Dittus-Boelter correlation. The transition region between low and high wall superheat uses an interpolation between nucleate and film boiling HTCs (by Bromley et al. [12] at low flow quality and by Groeneveld and Snoek [13] at high flow quality) using scaling laws by Ramilison and Leinhard [14]. At high wall superheats, either Bromley or Groeneveld correlations are used for low flow quality or high flow quality, respectively. The user does not have direct access to these subroutines that govern the flow boiling, although certain variables can be changed such as XNB, the cut-off value for low flow and high flow quality. Although a parametric analysis can be run on this and other user-controlled variables to match existing datasets, it is not useful for purposes of evaluating the predictive capability of the Built-In Correlations. Therefore, the default values were used to compare performance of the Built-In Correlations compared to the new universal correlations.

The new universal correlations were ported into Thermal Desktop using an input into a User Code element in the Logic Block. The code takes the inlet and operating conditions of the run and outputs the HTC at each data point as well as the predicted location of z_{CHF}. Then at each iteration, Thermal Desktop takes the inlet and operating conditions and new universal correlations for HTC and computes the fluid states, pressure drop, axial conduction, and wall temperatures as outlined in Figure 2. The original version of the universal code developed in MATLAB [2] contained calculations for pressure drop and axial conduction, but these two were not ported over into Thermal Desktop and are not part of the User Code. Instead, the built-in pressure drop and axial conduction methods were used.

Table 2: Built-In Thermal Desktop flow boiling correlation breakdown

	Low Flow Quality (x < XNB)	High Flow Quality (XNB < x < 1.0)
Low Wall Superheat (below T_{CHF})	Chen [11]	Linear interpolation between Chen [11] and Dittus-Boelter
Transition (above T_{CHF} and the Smaller of T_{leid} and T_{dfb})	Non-linear interpolation between nucleate and film boiling using scaling laws	Non-linear interpolation between nucleate and film boiling using scaling laws by Ramilison and Leinhard [14]

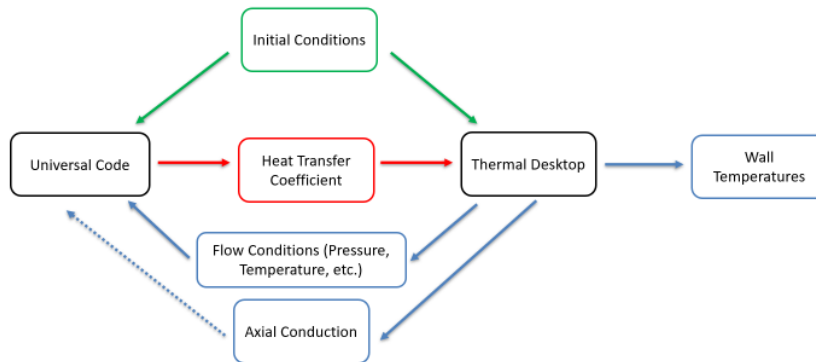|	by Ramilison and Leinhard [14]	
High Wall Superheat (above T_{CHF} and the smaller of T_{leid} and T_{dfb})	Bromley et al. [12]	Groeneveld and Snoek [13]

Figure 2: Flow diagram of Thermal Desktop and Universal Code

3.3. Calculated Versus Fixed z_{CHF}

Two versions of the code were developed for use in Thermal Desktop in order to fully demonstrate the ability of the universal correlations to correctly predict HTCs. The original version, called Calculated z_{CHF}, predicts the HTC for all points in the test section but also the location of z_{CHF}. Therefore, any error in z_{CHF} will compound error in the region where the boiling regime in the model does not match that of the data. For example, if the model predicts z_{CHF} far upstream of where it actually occurs in the data, a significant portion of the model will predict film boiling where the data shows nucleate boiling. Because film boiling wall temperatures can be significantly higher than nucleate boiling wall temperatures, the error in this region of the test significantly skew the results because of the mismatch in the boiling regimes. Therefore, a second Thermal Desktop model, called Fixed z_{CHF}, was run where the experimental z_{CHF} location from Table 1 was fed into the model as an input so that the flow boiling regime between model and data always matched. This second model offers a true demonstration of the ability of the new universal correlations to predict the HTCs and resultant wall temperatures in the correct flow boiling regime. Of note is that the z_{CHF} location cannot be fixed in the Built-In model using the built-in correlations, so the results for a fixed Built-In model are not shown. Note that 4 of the 10 runs list no experimental z_{CHF} (see Table 1), which indicates that the transition to film boiling occurs either beyond the location of the last thermocouple or past the end of the test section itself.

4. Results and Discussion

The predicted wall temperature along the axis of the pipe was compared to each of the 10 runs. For each run, two different error metrics were calculated, mean average percentage error (MAPE) and symmetric mean average percentage error (SMAPE) shown in Equations 2 and 3. Here, n represents the number of data points, A_t is the actual data value, and F_t is the predicted value. The MAPE

penalizes overprediction of the wall temperature more so than underprediction, whereas the SMAPE weights both errors equally.

$$MAPE = \frac{1}{n}\sum_{t=1}^{n}\left|\frac{F_t - A_t}{A_t}\right| \tag{2}$$

$$SMAPE = \frac{1}{n}\sum_{t=1}^{n}\left|\frac{F_t - A_t}{(A_t + F_t)/2}\right| \tag{3}$$

The error in z_{CHF} is calculated as the difference between the predicted and actual experimental z_{CHF} location over the heated length of the entire test section:

$$z_{CHF}\ error = \left|\frac{z_{CHF,predicted} - z_{CHF,actual}}{L_H}\right| \tag{4}$$

For cases where the model predicts z_{CHF} before the first data point but the data shows z_{CHF} beyond the last data point, an error of 100% is used. Tables 3 and 4 present compiled results for the Calculated z_{CHF} models and Fixed z_{CHF} models, respectively. Parity plots are presented in Figures 3-7 for each of the Calculated and Fixed z_{CHF} models. The Calculated z_{CHF} parity plot compares all data points from the new universal correlations and the Built-In correlations. The metrics θ and φ show the percentage of predicted values that lie within +/- 30% and +/- 50% of the experimental values, respectively. For the Fixed z_{CHF} case, two separate parity plots are given, showing separately the pre- and post-CHF values.

Overall, the new universal correlations perform substantially better than Thermal Desktop's built-in correlations. For the Calculated z_{CHF} model where the new correlations predict both HTCs and z_{CHF} location, the wall temperature is predicted within an average of 13.3% MAPE and 13.5% SMAPE across the entire length of the pipe, whereas the built-in correlations predict wall temperatures within an average of 71% MAPE and 49% SMAPE. Additionally, the universal correlations were able to predict the z_{CHF} location within 20% for 9 out of the 10 cases whereas the built-in correlations predicted z_{CHF} significantly upstream of the data in all cases, with an average error of 85.0%. When comparing the Fixed z_{CHF} model to the data, the new universal correlations can predict pre-CHF wall temperatures within an average of 6% and post-CHF temperatures within 31% SMAPE. Overall, the new universal correlations demonstrate superior predictive performance over the baseline correlations for this LHe validation case, predicting wall temperature better by an average factor of 4 over the baseline correlations.

Table 3: Compiled results for Calculated z_{CHF} models

Run # from [1]	Universal Correlations MAPE (%)	Universal Correlations SMAPE (%)	Universal Correlations z_{CHF} Error (%)	Built-In Correlations MAPE (%)	Built-In Correlations SMAPE (%)	Built-In Correlations z_{CHF} Error (%)
Figure 3 Run 1	22.5%	18.0%	18.8%	107.4%	67.9%	89.4%
Figure 3 Run 2	14.6%	11.1%	21.1%	99.2%	66.3%	100.0%
Figure 4	3.4%	3.7%	8.3%	129.8%	75.5%	96.8%
Figure 5	1.1%	1.1%	0.0%	71.0%	52.4%	100.0%
Figure 6	5.7%	6.0%	0.0%	8.8%	9.2%	100.0%
Figure 7	23.1%	27.9%	64.3%	31.5%	25.8%	37.1%

Figure 8	14.1%	14.4%	13.2%	76.6%	53.9%	89.6%
Figure 9	21.7%	27.7%	5.1%	80.7%	59.1%	68.7%
Figure 9	4.1%	4.0%	2.7%	75.3%	54.7%	100.0%
Figure 10	23.1%	21.1%	6.3%	27.5%	24.0%	68.9%
Average	**13.3%**	**13.5%**	**14.0%**	**70.8%**	**48.9%**	**85.0%**

Table 4: Compiled results for Fixed z_{CHF} model

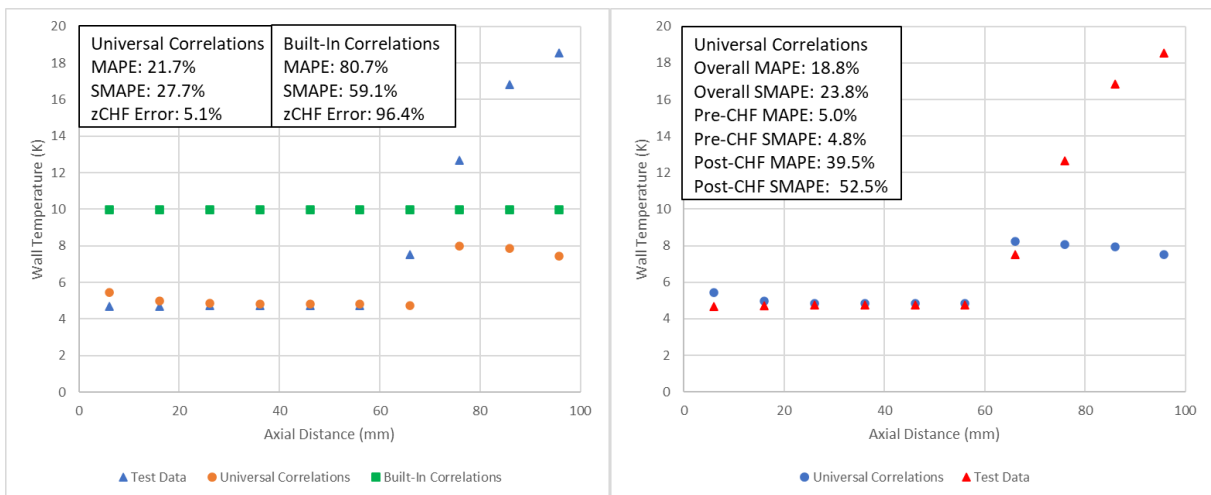| Run # from [1]	Universal Correlations pre-CHF MAPE (%)	Universal Correlations pre-CHF SMAPE (%)	Number of pre-CHF data points	Universal Correlations post-CHF MAPE (%)	Universal Correlations post-CHF SMAPE (%)	Number of post-CHF data points
Figure 3 Run 1	1.0%	1.0%	8	23.7%	29.7%	2
Figure 3 Run 2	0.8%	0.8%	10	-	-	-
Figure 4	5.9%	7.4%	10	-	-	-
Figure 5	1.1%	1.1%	10	-	-	-
Figure 6	5.7%	6.0%	10	-	-	-
Figure 7	8.3%	7.9%	3	26.0%	24.5%	7
Figure 8	10.8%	9.9%	8	25.2%	20.2%	2
Figure 9	5.0%	4.8%	6	39.5%	52.5%	4
Figure 9	3.5%	3.3%	10	-	-	-
Figure 10	18.7%	17.5%	7	31.2%	27.7%	3
Average	**5.5%**	**5.5%**	**-**	**29.5%**	**31.3%**	**-**

Figure 3: Experimental versus predicted wall temperature as a function of distance along the pipe for Figure 9 from Giarrantano et al. [1] for Calculated z_{CHF} (Left) and Fixed z_{CHF} (Right)
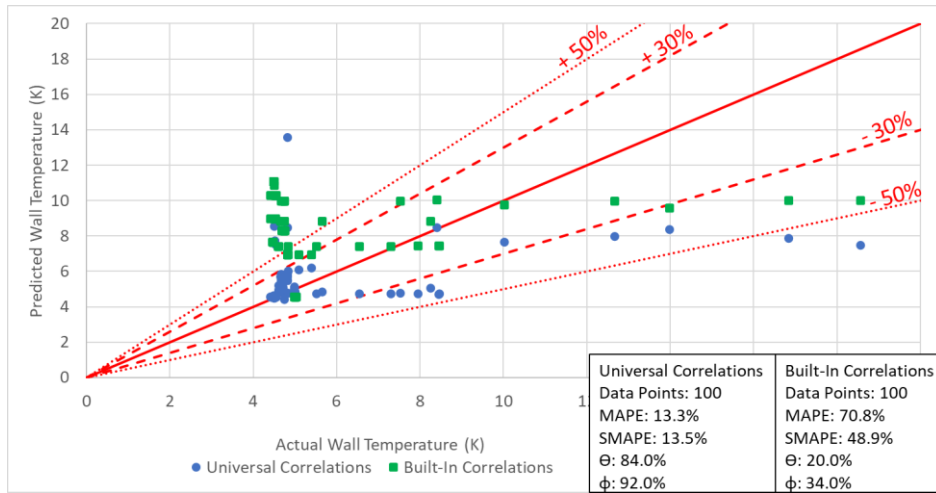
Figure 5: Parity Plot of all Universal Correlations and Built-In Correlations Data Points for Giarrantano et al. [1], Calculated z_{CHF}
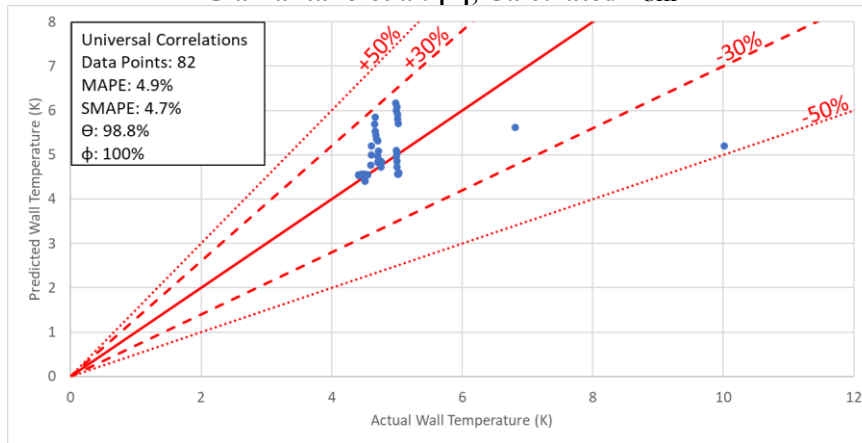

Figure 6: Parity Plot of Universal Correlations and Built-In Correlations for Pre-CHF for Giarrantano et al. [1], Fixed z_{CHF}
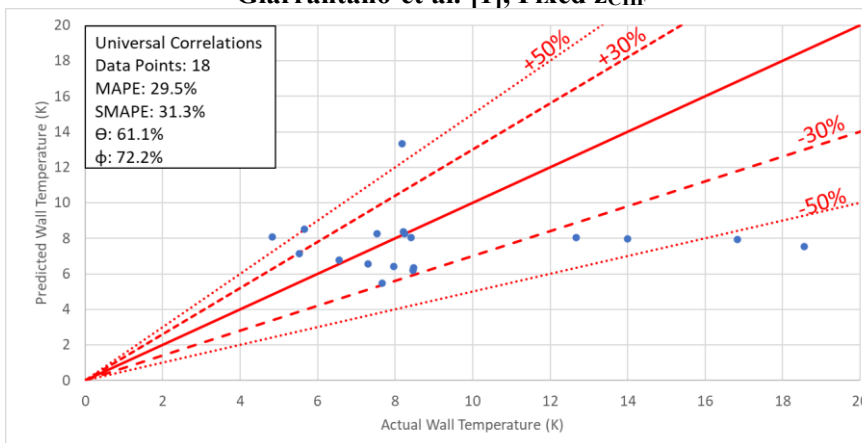

Figure 7: Parity Plot of Universal Correlations and Built-In Correlations for Post-CHF for Giarrantano et al. [1], Fixed z_{CHF}

5. Conclusion

A set of new universal correlations were developed for cryogenic flow boiling and implemented into Thermal Desktop, showing substantial improvement over the existing built-in correlations, predicting

wall temperature with an SMAPE value of nearly 4 times lower and location of z_{CHF} of 6 times lower for this liquid helium flow boiling validation case. Concurrent work includes validation against other historical datasets for other cryogens to test the validity of the new correlations. Adoption of these new universal correlations into Thermal Desktop will improve existing predictive models for cryogenic flow boiling for design of future spaceflight missions.

6. References

[1] Giarrantano, P. J., Hess, R.C., & Jones, M.C. Forced Convection Heated Transfer to Subcritical Helium I. Interim Report Prepared for Air Force Aero Propulsion Laboratory, NBSIR 73-322, 1973.

[2] Hartwig, J.W., Ganesan, V., Johnson, A., "A Continuous Flow Boiling Curve in the Heating Configuration Based on New Cryogenic Universal Correlations" Int. J. of Heat and Mass Transfer 2024b.

[3] Ganesan, V., Patel, R., Hartwig, J., & Mudawar, I. Universal critical heat flux (CHF) correlations for cryogenic flow boiling in uniformly heated tubes. International Journal of Heat and Mass Transfer, 166, 120678, 2021.

[4] Ganesan, V., Patel, R., Hartwig, J., & Mudawar, I. Review of databases and correlations for saturated flow boiling heat transfer coefficient for cryogens in uniformly heated tubes, and development of new Consolidated Database and universal correlations. International Journal of Heat and Mass Transfer, 179, 121656. https://doi.org/10.1016/j.ijheatmasstransfer.2021.121656, 2021.

[5] Ganesan, V., Patel, R., Hartwig, J., and Mudawar, I. Universal correlations for post-CHF saturated and superheated flow film boiling heat transfer coefficient, minimum heat flux and rewet temperature for cryogenic fluids in uniformly heated tubes. International Journal of Heat and Mass Transfer, 195, 123054. https://doi.org/10.1016/j.ijheatmasstransfer.2022.123054, 2022.

[6] Ganesan, V., Patel, R., Hartwig, J.W., and Mudawar, I. "Development of Two-Phase Frictional Pressure Gradient Correlations for Saturated Cryogenic Flow Boiling in Uniformly Heated Tubes" International Journal of Heat and Mass Transfer 2024.

[7] Ganesan, V., Patel, R., Hartwig, J.W., and Mudawar, I. "Universal correlations for pre-CHF subcooled boiling heat transfer coefficient and wall superheat for onset of nucleate boiling for cryogenic fluids in uniformly heated tubes." Int. J. Heat Mass Trans. 2024.

[8] Mercado, M., Wong, N., Hartwig, J. "Assessment of two-phase heat transfer coefficient and critical heat flux correlations for cryogenic flow boiling in pipe heat experiments." International Journal of Heat and Mass Transfer, 133, pp 295-315, 2019.

[9] C&R Technologies. TD Suite Manual For Thermal Desktop, TD Direct, and SINDA/FLUINT. Version 6.3, Thermal Desktop Patch 13, SINDA/FLUINT Patch 10, 2022.

[10] Mercado, M., Tesny, E., Hartwig, J., et al. "Validation of Universal Cryogenic Flow Boiling Correlations in Thermal Desktop for Liquid Methane and Liquid Nitrogen." Proceedings from the 30th Space Cryogenics Workshop, Kailua-Kona, HI, 2023.

[11] Chen, J.C. "Correlation for Boiling Heat Transfer to Saturated Fluids in Convective Flow" Industrial & Engineering Chemistry Process Design and Development 5, 322 – 329. 1966.

[12] Bromley, J., LeRoy, N., and Robbers, J. "Heat Transfer in Forced Convection Film Boiling," Industrial and Engineering Chemistry, p. 2639, 1953.

[13] Groeneveld, D. and Snoek, C. "A Comprehensive Examination of Heat Transfer Correlations Suitable for Reactor Safety Analysis," Multiphase Science and Technology, 1986.

[14] Ramilson, J. and Lienhard, J. "Transition Boiling Heat Transfer and the Film Transition Regime," Journal of Heat and Mass Transfer, vol. 109, 1987.